**INNOVATION IN METALLURGICAL INDUSTRIAL AND LABORATORY EQUIPMENT, TECHNOLOGIES AND MATERIALS**

**ИННОВАЦИИ В МЕТАЛЛУРГИЧЕСКОМ ПРОМЫШЛЕННОМ И ЛАБОРАТОРНОМ ОБОРУДОВАНИИ, ТЕХНОЛОГИЯХ И МАТЕРИАЛАХ**

**UDC** 621.791.754.3
**DOI** 10.17073/0368-0797-2025-6-626-635



***Original article***
***Оригинальная статья***

# Analysis of processing 40Kh13 martensitic stainless steel billet obtained by wire electron beam additive manufacturing

**C. Zhang[1], V. N. Kozlov[1], D. A. Chinakhov[2], V. A. Klimenov[1], R. V. Chernukhin[2]**

[1] **National Research Tomsk Polytechnic University** (30 Lenina Ave., Tomsk 634050, Russian Federation)
[2] **Novosibirsk State Technical University** (20 Karla Marksa Ave., Novosibirsk 630073, Russian Federation)

cinzhun1@tpu.ru

***Abstract***. The authors investigated the microstructure and mechanical properties of the samples obtained by the method of wire electron beam additive manufacturing (WEBAM), and their machinability by milling forces using the Taguchi method. Grains of previous austenite and annealed martensite were observed in the samples in various directions. The grains of the previous austenite grow along the surfacing direction and exhibit a pronounced orientation. On the lateral surface of the sample, the grains of the previous austenite are columnar, their hardness is approximately 505 $HV_{0.1}$. On the upper surface of the sample, the grains of the previous austenite are isometric, their hardness is approximately 539 $HV_{0.1}$. The degree of transformation into martensite varies in different parts of the sample. In the part close to the lateral surface, martensite is shallower and the previous austenitic grain boundaries are not observed. Its hardness is approximately 514 $HV_{0.1}$. In the lower part of the sample, due to multiple thermal cycles, martensite decomposes, while its hardness is low and is approximately 480 $HV_{0.1}$. In the upper part of the sample, martensite and the previous austenitic grain boundaries are observed, the hardness is approximately 513 $HV_{0.1}$. Due to the high hardness of the sample during climb milling, a stronger impact of the cutting edge on the sample leads to an increase in cutting force. Due to the low plasticity of the sample during conventional milling, a decrease in the volume of material pressed into the back surface of the tool leads to a decrease in cutting force. As the feed rate to the tooth increases, deformation of the material increases, the temperature increases, which leads to a decrease in the material strength. Reducing the material strength slows down the growth of cutting force.

***Keywords:*** electron beam additive manufacturing, microstructure, hardness, machinability, martensitic stainless steel, Taguchi method

***For citation:*** Zhang C., Kozlov V.N., Chinakhov D.A., Klimenov V.A., Chernukhin R.V. Analysis of processing 40Kh13 martensitic stainless steel billet obtained by wire electron beam additive manufacturing. *Izvestiya. Ferrous Metallurgy*. 2025;68(6):626–635. https://doi.org/10.17073/0368-0797-2025-6-626-635

# Анализ процесса обработки заготовки из мартенситной нержавеющей стали 40Х13, полученной методом проволочного электронно-лучевого аддитивного производства

**Ц. Чжан[1], В. Н. Козлов[1], Д. А. Чинахов[2], В. А. Клименов[1], Р. В. Чернухин[2]**

[1] **Национальный исследовательский Томский политехнический университет** (Россия, 634050, Томск, пр. Ленина, 30)
[2] **Новосибирский государственный технический университет** (Россия, 630073, Новосибирск, пр. Карла Маркса, 20)

cinzhun1@tpu.ru

***Аннотация***. Авторы исследовали микроструктуру и механические свойства образцов, полученных методом проволочного электронно-лучевого аддитивного производства (WEBAM), и их обрабатываемость по силам фрезерования с использованием метода Тагучи. В образцах в различных направлениях наблюдались зерна предыдущего аустенита и отожженный мартенсит. Зерна предыдущего аустенита растут вдоль направления наплавки и демонстрируют выраженную ориентацию. На боковой поверхности образца зерна предыдущего аустенита являются столбчатыми, их твердость составляет примерно 505 $HV_{0,1}$. На верхней поверхности образца зерна предыдущего аустенита являются изометрическими, их твердость составляет примерно 539 $HV_{0,1}$. В разных частях образца степень превращения в мартенсит различается. В части, близкой к боковой поверхности, мартенсит более мелкий и предыдущие аустенитные межзеренные границы не наблюдаются. Его твердость составляет примерно 514 $HV_{0,1}$. В нижней части образца, вследствие множественных термоциклов, происходит разложение мартенсита, при этом его твердость низкая и составляет примерно 480 $HV_{0,1}$. В верхней части образца наблюдаются мартенсит и предыдущие аустенитные межзеренные границы, твердость составляет примерно 513 $HV_{0,1}$. Из-за высокой твердости образца при попутном фрезеровании более сильный удар режущей кромки о образец приводит к увеличению силы резания. Вследствие низкой пластичности образца при встречном фрезеровании уменьшение объема материала, вдавливаемого в заднюю поверхность инструмента, приводит к снижению силы резания. При увеличении скорости подачи на зуб деформация материала увеличивается, температура повышается, что приводит к снижению прочности материала и, соответственно, замедляет рост силы резания.

***Ключевые слова:*** проволочное электронно-лучевое аддитивное производство, микроструктура, твердость, обрабатываемость, мартенситная нержавеющая сталь, метод Тагучи

***Для цитирования:*** Чжан Ц., Козлов В.Н., Чинахов Д.А., Клименов В.А., Чернухин Р.В. Анализ процесса обработки заготовки из мартенситной нержавеющей стали 40Х13, полученной методом проволочного электронно-лучевого аддитивного производства. *Известия вузов. Черная металлургия*. 2025;68(6):626–635. https://doi.org/10.17073/0368-0797-2025-6-626-635

## Introduction

In recent years, wire electron beam additive manufacturing (*Wire Electron Beam Additive Manufacturing* – WEBAM) has attracted growing interest because it combines a high deposition rate (up to 2500 $cm^3/h$) with the ability to produce parts that show high strength and fatigue resistance [1 – 6]. The process is also flexible from a manufacturing standpoint: it can operate with wire diameters down to 0.5 mm and can be used to obtain materials with a prescribed phase content, for example in nickel–aluminum alloy systems [7].

However, in contrast to conventional casting and forging, thermal processes in additive manufacturing are more complex, resulting in uncertainty in the mechanical properties of printed parts. For example, studies on 10Kh12N10T stainless steel reported that increased strength is associated with a high density of dislocations and intermetallic compounds concentrated at interlayer boundaries [8]. A study of heat dissipation conditions during the deposition of 308LSi steel showed that the use of copper as a cooling medium results in hardness values approximately 5 % higher than those obtained with air, while the hardness of the upper part of the sample is about 8 % higher than that of the lower part [9]. When thin-walled parts are produced, a columnar crystalline structure tends to develop, which leads to pronounced anisotropy; the strength difference between longitudinal and transverse directions can reach 70 MPa [10]. Due to the high heat input, WEBAM-produced parts exhibit inferior as-built surface quality, which adversely affects subsequent conventional machining operations such as milling and turning [11; 12]. 40Kh13 martensitic stainless steel (an analogue of AISI 420) is widely used for large, complex-shaped parts because it is relatively inexpensive while offering moderate corrosion resistance and high strength. At the same time, its high hardness limits machinability and accelerates tool wear [13]. In addition, because martensitic steels are highly sensitive to temperature variations and because the thermal gradient during deposition is strongly directional, WEBAM-built samples often exhibit anisotropy in both microstructure and mechanical properties [14; 15]. As a result, machining of such martensitic steels becomes even more uncertain.

The *Taguchi method* applied in this study is an approach to experimental optimization that uses the *signal-to-noise ratio* (SNR) together with *orthogonal arrays* to identify an optimal combination of parameters [16 – 20].

The present work therefore focuses on the microstructure and microhardness of WEBAM-deposited 40Kh13 martensitic stainless steel in different directions and regions, and evaluates machinability using the Taguchi method.

## Materials and methods

The samples were produced by wire electron beam additive manufacturing on equipment designed and manufactured at Tomsk Polytechnic University. A filler wire with a diameter of 1.2 mm made of 40Kh13 martensitic stainless steel was used as the feedstock. The chemical composition of the wire was as follows (wt. %: 0.41 C, 13.2 Cr, 0.53 Si, 0.51 Ni, 0.49 Mn, 0.017 S, 0.021 P, with iron as the balance. The substrate was manufactured from the same material (40Kh13 steel). The dimensions of the samples were 70×15×14 mm (length×width×height). The printing parameters were as follows: accelerating voltage of 40 kV, beam current of 21 mA, scanning beam diameter of 3 – 5 mm, wire feed rate of 1050 mm/min, and wire feeding angle of 45°. The deposition process was carried out in a vacuum at a pressure of $5 \cdot 10^{-3}$ Pa.

Microstructural analysis was performed using a BIOMED MMP-1 metallographic microscope and by scanning electron microscopy with a JEOL JSM-6000 microscope. Microhardness measurements were conducted using an EMCO-TEST DuraScan-10 hardness tester, with a load holding time of 10 s.

The machinability of the samples was evaluated based on milling forces. Machining experiments were carried out on a CNC EMCO CONCEPT Mill 155 machine. Cutting forces were measured using a Kistler 9257 V dynamometer (Switzerland). In the dynamometer software (originally intended for turning-force measurements), the force components are displayed as $F_x$, $F_y$ and $F_z$. In the present milling tests, these components were interpreted as the milling-force components $P_h$, $P_v$ и $P_x$, respectively (Fig. 1). For machining, an end milling cutter with a diameter of 8 mm and four teeth, manufactured by GESAC, was used. The helix angle (ω) of the milling cutter was 35°, while the rake angle (γ) and clearance

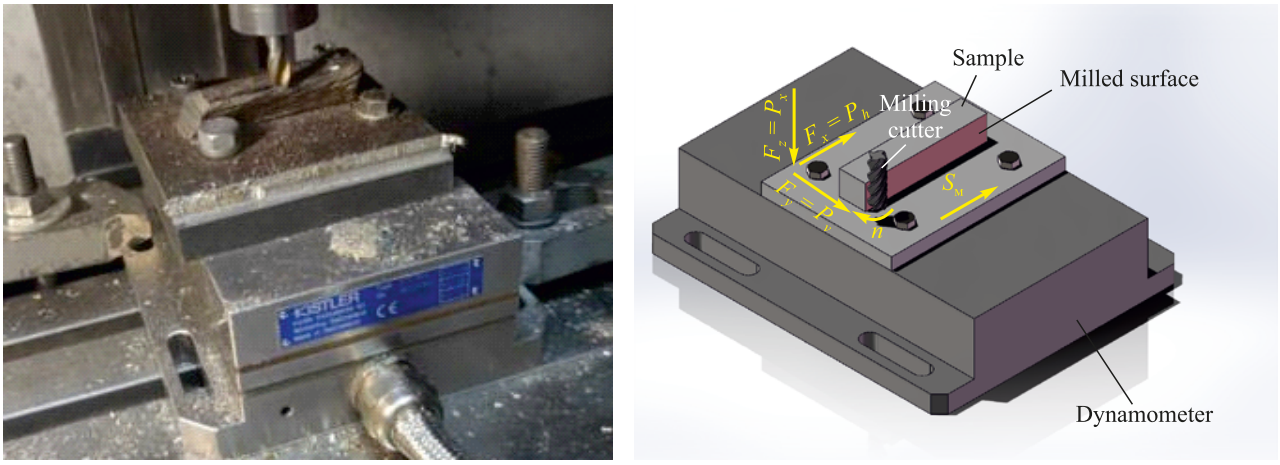


*a* *b*

***Fig. 1.*** Appearance (*a*) and model (*b*) of the dynamometer, milling cutter and sample installation

***Рис. 1.*** Внешний вид (*a*) и модель (*b*) установки динамометра, фрезы и образца

*Table 1.* **Experimental levels of the factors**

*Таблица 1.* **Экспериментальные уровни факторов**

| Factor | Level | | |
|---|---|---|---|
| | *1* | *2* | *3* |
| *A*: milling scheme | Climb milling (Cl) | Conventional milling (Con) | |
| *B*: feed rate $s_m$, mm/min | 56 | 28 | 5,6 |
| *C*: milling cutter rotational speed *n*, rpm | 2000 | 1000 | 500 |

angle (α) were 7° and 5°, respectively. The base material of the milling cutter was VK8 cemented carbide (92 % tungsten carbide and 8 % cobalt as a binder). The surface of the milling cutter was coated with a wear-resistant AlCrSiN coating.

The experimental levels of the factors are presented in Table 1.

To determine the minimum milling force, the signal-to-noise ratio $S/N(\eta)$ was used:

$$S/N(\eta) = -10\lg\left(\frac{1}{j}\sum_{i=1}^{j} P_i^2\right), \quad (1)$$

where $P_i$ is the force value measured during the $i$-th milling pass.

The mean milling force $P_{avg}$ was calculated using the following expression:

$$P_{avg} = \frac{1}{x}\sum_{i=1}^{x} P_i, \quad (2)$$

where $x$ is the number of experimental repetitions.

## Results and discussion

### Analysis of the microstructure and mechanical properties of the sample in different directions

As shown in Fig. 2, the *OZ* axis corresponds to the deposition build direction, the *OY* axis is oriented along the weld bead, and the *OX* axis represents the transverse direction relative to the weld bead.

At low magnification, the *XOZ* and *YOZ* planes reveal austenite grains prior to the martensitic transformation (previous austenite grains), which exhibit a columnar morphology with their long axes aligned along the *OZ* direction. This behavior is associated with the thermal conditions during deposition: the lower layers experience multiple thermal cycles and accumulate heat, resulting in the formation of a dominant heat flow opposite to the deposition direction (i.e., opposite to the *OZ* axis). As a consequence, a pronounced preferential growth orientation of the previous austenite grains develops along the *OZ* axis. In contrast, grains observed on the *XOY* plane display an equiaxed morphology. This can be attributed to the high deposition rate combined with relatively low heat input, which suppresses grain growth along the *OY* direction and equalizes heat dissipation conditions along the *OX* and *OY* directions. This promotes equal grain growth rates along the *OX* and *OY* directions, resulting in the formation of equiaxed grains. In addition, while the degree of corrosion within individual previous austenite grains is nearly uniform, noticeable differences are observed between different grains. This behavior may be related to variations in the extent and morphology of martensitic transformations caused by elemental segregation under the high cooling rates characteristic of the deposition process [15].

Fig. 2, *b* clearly shows that a large number of needle-like or plate-like martensitic structures formed within the previous austenite grains as a result of a diffusionless phase transformation.

The martensite within these grains is distributed in the form of an interwoven network. The orientation of martensite varies significantly from one austenite grain to another. Furthermore, a pronounced transgranular phenomenon is observed at the boundaries of previous austenite grains, which may be associated with local stress concentrations or energy gradients. In the *YOZ* and *XOZ* planes, the sizes of the previous austenite grains are nearly identical, further confirming the similarity of temperature

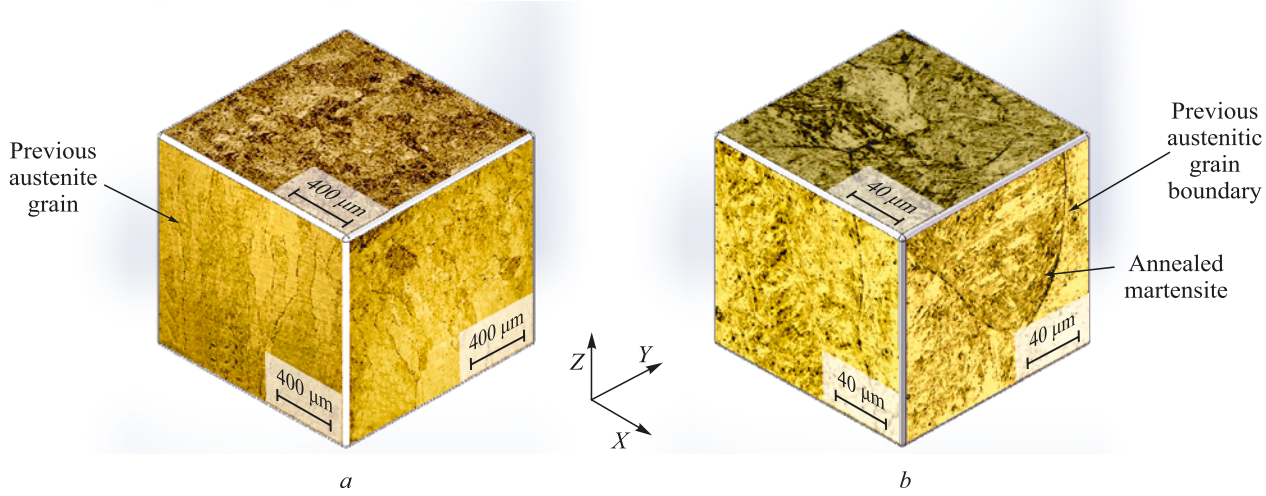


***Fig. 2.*** Microstructure of the samples deposited by WEBAM in different planes at low (*a*) and high (*b*) magnification

***Рис. 2.*** Микроструктура образцов, наплавленных методом WEBAM, в разных плоскостях при малом (*a*) и большом (*b*) увеличении

gradients along the *OX* and *OY* directions. In contrast, the smaller size of previous austenite grains in the *XOY* plane leads to a denser martensitic network with a shorter average length of martensitic features. This difference can be explained by faster cooling along the *OX* and *OY* directions or by the formation of more pronounced compositional gradients in this plane due to elemental segregation, which suppresses grain coarsening [21]. As a result, the frequency of transgranular phenomena at grain boundaries in the *XOY* plane is also reduced.

A scanning electron microscopy image of the sample microstructure in the *XOZ* plane is presented in Fig. 3. Plate-like martensite and carbides are clearly visible. The measured hardness of the sample in the *XOZ* plane is 504.67 $HV_{0.1}$, which is significantly lower than that of quenched martensite (750 HV) [21]. However, the thickness of the plate-like martensitic layer is relatively small, amounting to 1.23 ± 0.56 μm. This reduction in hardness can be explained by the fact that the sample underwent several thermal cycles, during which martensite experienced thermal activation and partial decomposition, leading to an increased fraction of retained austenite. During the deposition of the first layer, the austenitic phase rapidly transforms into quenched martensite owing to the high cooling rate, resulting in the maximum martensite content. However, when the second or third layer is deposited, the first layer remains within the heat-affected zone. This promotes carbon diffusion at martensite – martensite or martensite – retained austenite interfaces, causing partial reversion of martensite to austenite. At the same time, chromium atoms impede carbon diffusion, thereby limiting martensite decomposition and restricting it to a partial transformation. Consequently, despite repeated thermal cycles, the hardness of the material remains significantly higher than that of austenitic steel [8].

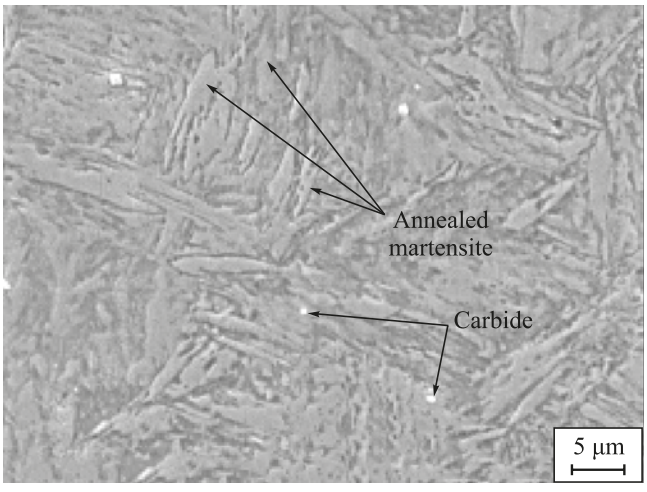


***Fig. 3.*** Microstructure of the sample deposited by WEBAM in *XOZ* plane observed using the scanning electron microscope

***Рис. 3.*** Микроструктура образца, наплавленного методом WEBAM в плоскости *XOZ*, наблюдаемая с помощью сканирующего электронного микроскопа

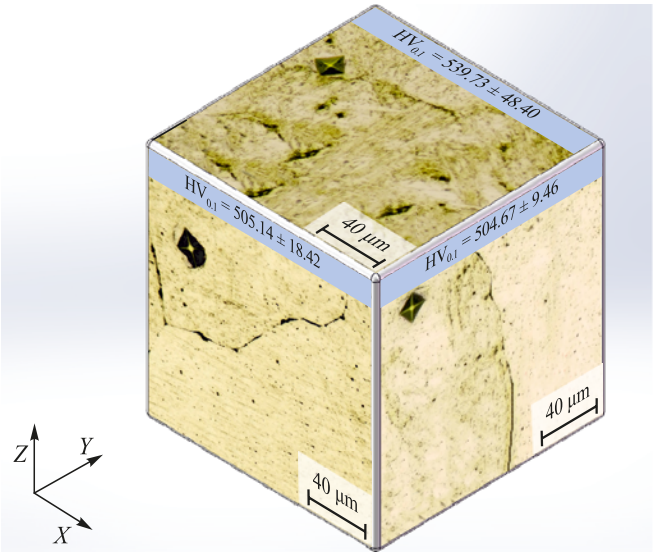


***Fig. 4.*** Microhardness of the sample deposited by WEBAM in different directions

***Рис. 4.*** Микротвердость образца, наплавленного методом WEBAM, в разных направлениях

The hardness of the sample in different directions is shown in Fig. 4. As noted above, the higher cooling rates along the *OX* and *OY* directions result in smaller previous austenite grain sizes in the *XOY* plane and a higher degree of martensitic transformation. This promotes the formation of a more continuous and homogeneous martensitic network in the *XOY* plane, which effectively impedes dislocation motion and increases the hardness to 539.73 $HV_{0.1}$. In contrast, the cooling rate along the *OZ* direction is lower, while temperature gradients along the *OX* and *OY* directions are similar. This leads to a lower degree of martensitic transformation in the *XOZ* and *YOZ* planes, facilitating dislocation motion and multiplication and promoting plastic deformation. As a result, the hardness values on these two planes are nearly identical, amounting to 505.14 and 504.67 $HV_{0.1}$, respectively.

## *Analysis of the microstructure in different parts of the sample*

Microstructural images obtained from different regions of the sample are shown in Fig. 5. In the region close to the lateral surface of the sample (Fig. 5, *a*), the previous austenitic grain boundaries are indistinct. The precipitated carbide inclusions are small, and the clusters of annealed martensite are fine and uniformly distributed. This behavior is attributed to more favorable heat dissipation conditions near the lateral surface, where the cooling rate is higher. The increased cooling rate promotes the formation of a large number of fine martensitic fea-

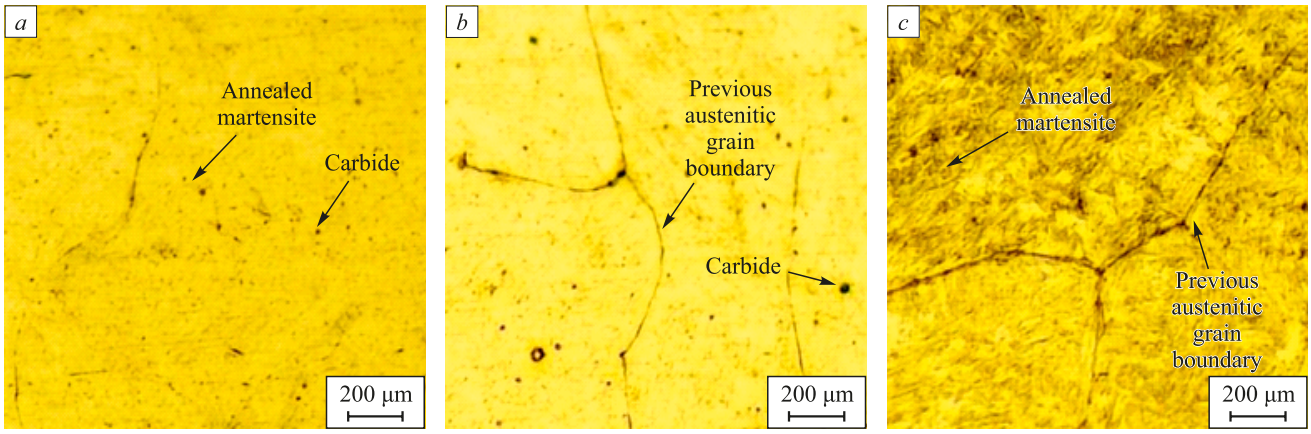


***Fig. 5.*** Microstructure of the sample deposited by WEBAM in *YOZ* plane in the part close to the lateral surface (*a*), in the lower part (*b*), and in the upper part (*c*)

***Рис. 5.*** Микроструктура образца, наплавленного методом WEBAM, в плоскости *YOZ* в части, близкой к боковой поверхности (*a*), в нижней части (*b*) и в верхней части (*c*)

tures. At the same time, rapid cooling enhances the manifestation of a transgranular phenomenon during the martensitic transformation, as a result of which the previous austenitic grain boundaries become blurred. In the lower part of the sample (Fig. 5, *b*), the previous austenitic grain boundaries are clearly visible, together with large carbide precipitates and a relatively small amount of martensite. This is explained by the lower cooling rate in the lower region compared with the area close to the lateral surface, which leads to a less pronounced transgranular phenomenon and, consequently, to clearly defined previous austenitic grain boundaries. In addition, because the lower part of the sample experienced a relatively larger number of thermal cycles during deposition, the amount of precipitated carbides and decomposed martensite increased. In the upper part of the sample (Fig. 5, *c*), the microstructure differs from both the lower region and the area close to the lateral surface. The previous austenitic grain boundaries and martensite are clearly visible, and the thickness of the martensitic layer is greater. This is associated with the smaller number of thermal cycles experienced by the upper part of the sample, which results in only limited martensite decomposition and allows its structure to remain well defined. At the same time, compared with the region near the lateral surface, the cooling rate in the upper part was lower, leading to the formation of a thicker martensitic layer.

Indentations obtained during microhardness measurements in different regions of the sample are shown in Fig. 6. The microhardness is lowest in the lower part of the sample due to martensite decomposition. In the region close to the lateral surface, the microhardness is slightly higher than that measured in the upper part of the sample; however, both values exceed the microhardness measured in the central region of the *YOZ* plane shown in Fig. 4. This can be explained by the higher

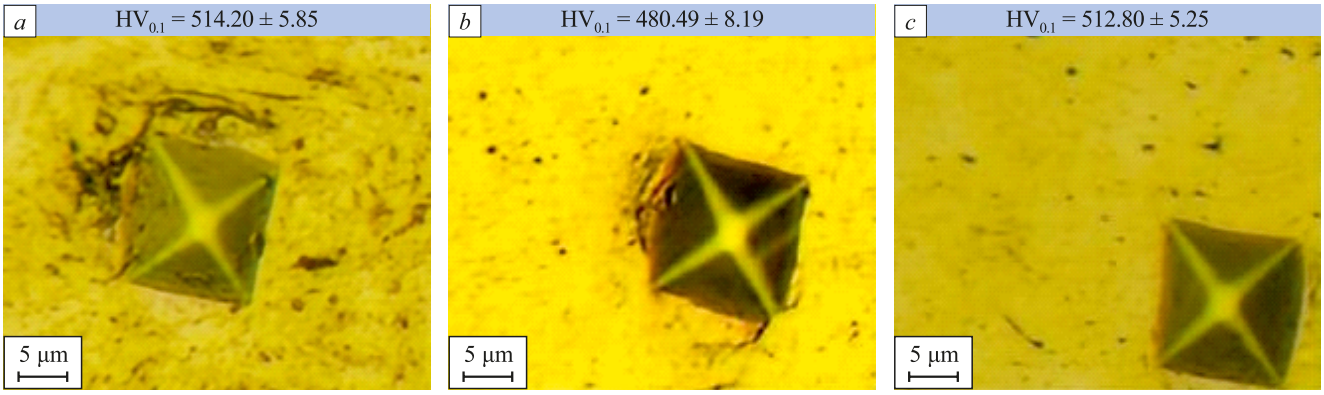


***Fig. 6.*** Microhardness of the sample deposited by WEBAM in *YOZ* plane in the part close to the lateral surface (*a*), in the lower part (*b*), and in the upper part (*c*)

***Рис. 6.*** Измерение микротвердости образца, наплавленного методом WEBAM, в плоскости *YOZ* в части, близкой к боковой поверхности (*a*), в нижней части (*b*) и в верхней части (*c*)

martensite content in the upper part of the sample and by the smaller size of martensitic regions near the lateral surface, both of which contribute to increased hardness. In addition, owing to the smaller size of the previous austenitic grains, the microhardness on the *XOY* plane is higher than that on the *YOZ* plane in the different parts of the sample.

## Analysis of machinability based on milling forces

Using the Taguchi method, the present study investigated the machinability of a 40Kh13 martensitic stainless steel sample produced by the WEBAM process during milling along the *OX* direction on the *XOZ* surface. Based on calculations using Eqs. (1) and (2), the mean values of the experimental results and the corresponding signal-to-noise ratios are presented in Table 2.

The expression used to calculate the mean signal-to-noise ratio is given by:

$$S/N_{\text{avg}} = \frac{1}{m}\sum_{i=1}^{m} S/N_j, \quad (3)$$

where $m$ is the number of parameter combinations at the same level of the given factor [19].

As follows from Tables 2 and 3, during climb milling the milling force $P_h$, acting along the feed direction, is lower than that obtained during conventional milling, whereas the force $P_v$, acting perpendicular to the feed direction, is higher than in conventional milling (Fig. 7). These differences arise because, when machining with a new milling cutter, the dominant tangential force $P_z$ (acting along the cutting speed $v$) during conventional milling is oriented almost along the feed direction, while during climb milling it is oriented nearly perpendicular to the feed direction [14]. In addition, owing to the high hardness of martensitic stainless steel, the impact force acting on the cutting edge during climb milling is higher, whereas during conventional milling the low plasticity of the material reduces the volume of material pressed

*Table 2.* **Mean values of experimental results and signal-to-noise ratio**

*Таблица 2.* **Средние значения экспериментальных результатов и отношение сигнал/шум**

| Machining parameters | | | Mean values of experimental results, N | | | Signal-to-noise ratio $S/N$, dB | | |
|---|---|---|---|---|---|---|---|---|
| $A$: milling strategy | $B$: $s_м$, mm/min | $C$: $n$, rpm | $P_{h_{avg}}$ | $P_{v_{avg}}$ | $P_{x_{avg}}$ | $S/N_{P_h}$ | $S/N_{P_v}$ | $S/N_{P_x}$ |
| Climb milling | 56 | 2000 | 52.11 | 146.10 | 22.87 | –34.33 | –43.29 | –27.18 |
| Climb milling | 28 | 1000 | 74.25 | 159.77 | 19.87 | –37.41 | –44.07 | –25.96 |
| Climb milling | 5.6 | 500 | 43.09 | 82.03 | 18.22 | –32.76 | –38.28 | –25.21 |
| Conventional milling | 56 | 500 | 212.12 | 181.89 | 26.09 | –46.53 | –45.19 | –28.33 |
| Conventional milling | 28 | 1000 | 122.06 | 115.01 | 17.45 | –41.73 | –41.21 | –24.84 |
| Conventional milling | 5.6 | 2000 | 63.24 | 22.09 | 8.25 | –36.02 | –26.88 | –18.35 |

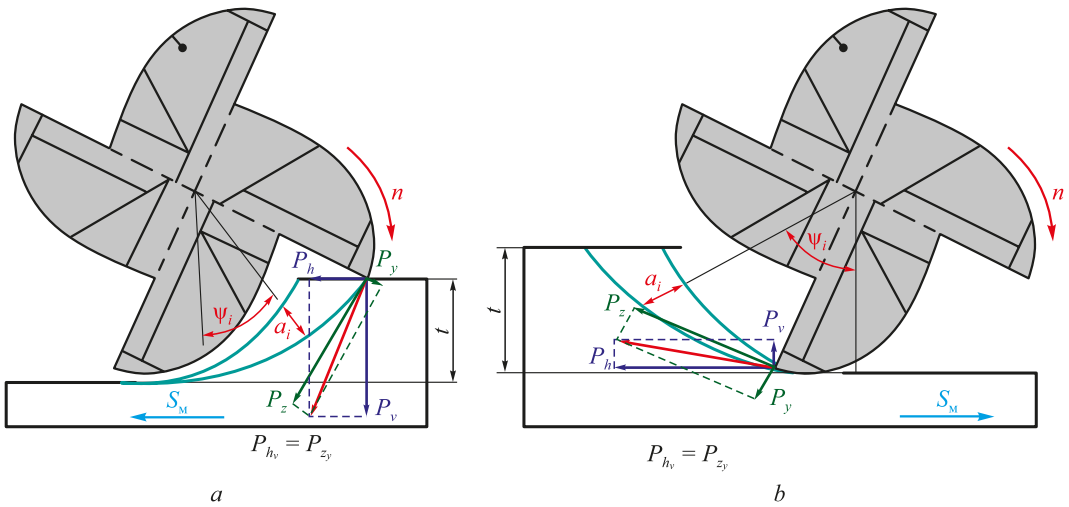


***Fig. 7.*** Direction of forces $P_h$, $P_v$, $P_z$ and $P_y$ during climb milling (*a*) and conventional milling (*b*)

***Рис. 7.*** Направление сил $P_h$, $P_v$, $P_z$ и $P_y$ при попутном фрезеровании (*a*) и при встречном фрезеровании (*b*)

*Table 3.* **Results of analysis of the factors effects on signal-to-noise ratio**

*Таблица 3.* **Результаты анализа влияния факторов на отношение сигнал/шум**

| Factor | Mean signal-to-noise ratio level $S/N_{P_{h_{avg}}}$, dB | | | Factor–signal-to-noise ratio plot for $P_h$ |
|---|---|---|---|---|
| | *1* | *2* | *3* | |
| *A*: milling scheme | –34.83 | –41.43 | – | 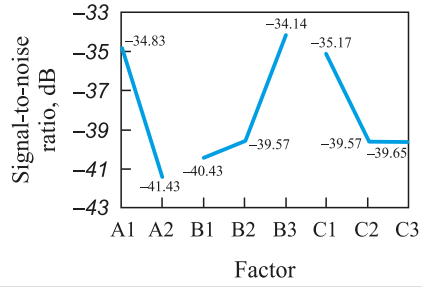 |
| *B*: feed rate $s_m$, mm/min | –40.43 | –39.57 | –34.14 | |
| *C*: rotational speed *n*, rpm | –35.17 | –39.57 | –39.65 | |
| Factor | Mean signal-to-noise ratio level $S/N_{P_{v_{avg}}}$, dB | | | Factor–signal-to-noise ratio plot for $P_v$ |
| | *1* | *2* | *3* | |
| *A*: milling scheme | –41.88 | –37.76 | – | 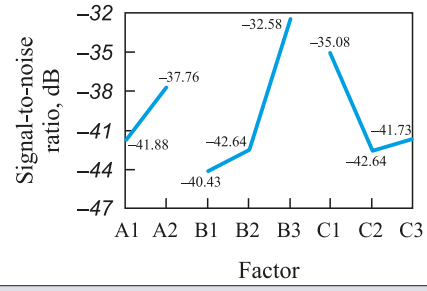 |
| *B*: feed rate $s_m$, mm/min | –40.43 | –42.64 | –32.58 | |
| *C*: rotational speed *n*, rpm | –35.08 | –42.64 | –41.73 | |
| Factor | Mean signal-to-noise ratio level $S/N_{P_{x_{avg}}}$, dB | | | Factor–signal-to-noise ratio plot for $P_x$ |
| | *1* | *2* | *3* | |
| *A*: milling scheme | –26.11 | –37.76 | – | 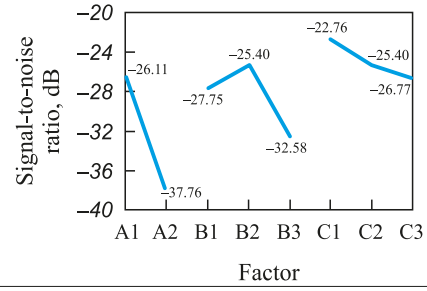 |
| *B*: feed rate $s_m$, mm/min | –27.75 | –25.40 | –32.58 | |
| *C*: rotational speed *n*, rpm | –22.76 | –25.40 | –25.77 | |

into the flank surface of the milling cutter, which leads to a decrease in the milling force.

As the feed rate $s_m$ increases, the chip thickness $a_i$ and material deformation increase, and the cutting temperature also rises. This results in an increase in the milling forces $P_h$ and $P_v$, however, the rate of their growth decreases. Moreover, an increase in cutting temperature may lead to martensite decomposition, which further reduces the material strength and additionally slows the growth of $P_h$ and $P_v$. When the rotational speed $n$ decreases, the feed per tooth $s_z$, increases, and consequently the chip thickness $a$ and material deformation increase; therefore, the milling forces $P_h$ and $P_v$ increase. According to the data in Table 2, the axial force $P_x$ shows little sensitivity to the feed rate $s_m$ and the rotational speed $n$, because is only weakly affected by chip thickness. However, due to temperature variations, the axial force $P_x$ may change slightly.

## Conclusions

In the present study, the microstructure and mechanical properties of the sample were investigated in different directions. On the lateral surface of the sample, columnar grains of previous austenite were observed, with a hardness of approximately 505 $HV_{0.1}$, whereas the upper surface exhibited equiaxed grains with a higher hardness of 539.73 $HV_{0.1}$. Overall, the microstructure of the sample corresponds predominantly to annealed martensite, within which a pronounced transgranular phe-

nomenon can be observed. This microstructural state is associated with the multiple thermal cycles experienced during deposition.

The microstructure and mechanical properties were also examined in different regions of the sample. In the region close to the lateral surface, the higher cooling rate results in finer martensitic features and increased hardness, reaching 514.2 ± 5.85 $HV_{0.1}$. In both the lower and upper regions of the sample, the previous austenitic grain boundaries are clearly visible. Because the lower part of the sample experienced a greater number of thermal cycles, martensite decomposition occurred, leading to a reduction in hardness to 480.49 ± 8.19 $HV_{0.1}$. In contrast, the upper part of the sample was subjected to fewer thermal cycles and retained a substantial amount of martensite; as a result, the hardness remained relatively high at 512.80 ± 5.25 $HV_{0.1}$.

The machinability of the sample was evaluated using the Taguchi method. Owing to the high hardness of the material, the impact of the cutting edge on the machined surface during climb milling leads to an increase in milling forces. Conversely, during conventional milling, the low plasticity of the material reduces the volume of material pressed into the flank surface of the milling cutter, resulting in lower milling forces. Furthermore, as the feed per tooth increases, the rise in cutting temperature reduces the material strength, which slows the growth of milling forces.

## References / Список литературы

1. Frazier W.E. Metal additive manufacturing: A review. *Journal of Materials Engineering and Performance*. 2014;23(6):1917–1928. https://doi.org/10.1007/s11665-014-0958-z
2. Klimenov V., Kolubaev E., Klopotov A., Chumaevskii A., Ustinov A., Strelkova I., Rubtsov V., Gurianov D., Han Z., Nikonov S., Batranin A., Khimich M. Influence of the coarse grain structure of a titanium alloy Ti-4Al-3V formed by wire-feed electron beam additive manufacturing on strain inhomogeneities and fracture. *Materials*. 2023;16(11):3901. https://doi.org/10.3390/ma16113901
3. Osipovich K., Kalashnikov K., Chumaevskii A., Gurianov D., Kalashnikova T., Vorontsov A., Zykova A., Utyaganova V., Panfilov A., Nikolaeva A., Dobrovolskii A., Rubtsov V., Kolubaev E. Wire-feed electron beam additive manufacturing: A review. *Metals*. 2023;13(2):279. https://doi.org/10.3390/met13020279
4. Negi S., Nambolan A.A., Kapil S., Joshi P.S., Manivannan E.R., Karunakaran K.P., Bhargava P. Review on electron beam based additive manufacturing. *Rapid Prototyping Journal*. 2020;26(3):485-498. https://doi.org/10.1108/RPJ-07-2019-0182
5. Kinsella M.E., Count P. Additive Manufacturing of Superalloys for Aerospace Applications (Preprint). AFRL-RX-WP-TP-2008-4318, 2008.
6. Mudge R.P., Wald N.R. Laser engineered net shaping advances additive manufacturing and repair. *Welding Journal*. 2007;86(1):44–48.
7. Astafurov S.V., Mel'nikov E.V., Astafurova E.G., Kolubaev E.A. Phase composition and microstructure of intermetallic alloys obtained using electron-beam additive manufacturing. *Izvestiya. Ferrous Metallurgy*. 2024;67(4):401–408. https://doi.org/10.17073/0368-0797-2024-4-401-408

   Астафуров С.В., Мельников Е.В., Астафурова Е.Г., Колубаев Е.А. Фазовый состав и микроструктура интерметаллических сплавов, полученных методом проволочного электронно-лучевого аддитивного производства. *Известия вузов. Черная металлургия*. 2024;67(4):401–408. https://doi.org/10.17073/0368-0797-2024-4-401-408
8. Kabaldin Yu.G., Chernigin M.A. Structure and its defects in additive manufacturing of stainless steels by laser melting and electric arc surfacing. *Izvestiya. Ferrous Metallurgy*. 2024;67(1):65–72. https://doi.org/10.17073/0368-0797-2024-1-65-72

   Кабалдин Ю.Г., Чернигин М.А. Структура и ее дефекты при аддитивном выращивании нержавеющих сталей методами лазерного спекания и электродуговой наплавки. *Известия вузов. Черная металлургия*. 2024;67(1):65–72. https://doi.org/10.17073/0368-0797-2024-1-65-72
9. Chinakhov D.A., Akimov K.O. Formation of the structure and properties of deposited multilayer specimens from austenitic steel under various heat removal conditions. *Metals*. 2022;12(9):1527. https://doi.org/10.3390/met12091527
10. Astafurova E.G., Panchenko M.Yu., Moskvina V.A., Maier G.G., Astafurov S.V., Melnikov E.V., Fortuna A.S., Reunova K.A., Rubtsov V.E., Kolubaev E.A. Microstructure and grain growth inhomogeneity in austenitic steel produced by wire-feed electron beam melting: the effect of post-building solid-solution treatment. *Journal of Materials Science*. 2020;55(22):9211–9224. https://doi.org/10.1007/s10853-020-04424-w
11. Tyagi P., Goulet T., Riso C., Stephenson R., Chuenprateep N., Schlitzer J., Benton C., Garcia-Moreno F. Reducing the roughness of internal surface of an additive manufacturing produced 316 steel component by chempolishing and electropolishing. *Additive Manufacturing*. 2019;25:32–38. https://doi.org/10.1016/j.addma.2018.11.001
12. Fox J.C., Moylan S.P., Lane B.M. Effect of process parameters on the surface roughness of overhanging structures in laser powder bed fusion additive manufacturing. *Procedia CIRP*. 2016;45:131–134. https://doi.org/10.1016/j.procir.2016.02.347
13. Rahman A.Z., Jauhari K., Al Huda M., Untariyati N.A., Azka M., Rusnaldy R., Widodo A. Correlation analysis of vibration signal frequency with tool wear during the milling process on martensitic stainless steel material. *Arabian Journal for Science and Engineering*. 2024;49:10573–10586. https://doi.org/10.1007/s13369-023-08397-1
14. Martyushev N.V., Kozlov V.N., Qi M., Tynchenko V.S., Kononenko R.V., Konyukhov V.Y., Valuev D.V. Production of workpieces from martensitic stainless steel using electron-beam surfacing and investigation of cutting forces when milling workpieces. *Materials*. 2023;16(13):4529. https://doi.org/10.3390/ma16134529
15. Alvarez L.F., Garcia C., Lopez V. Continuous cooling transformations in martensitic stainless steels. *ISIJ International*. 1994;34(6):516–521. https://doi.org/10.2355/isijinternational.34.516
16. Park S.H. Robust Design and Analysis for Quality Engineering. London: Chapman and Hall; 1996:256.

**17.** Unal R., Dean E.B. Taguchi approach to design optimization for quality and cost: An overview. In: *Proceedings of the Int. Society of Parametric Analyst 13th Annual. 1991, May 21–24*. 1991:1–10.
**18.** Phadke M.S. Quality Engineering Using Robust Design. Englewood Cliffs, NY: Prentice-Hall; 1989:320.
**19.** Günay M., Yücel E. Application of Taguchi method for determining optimum surface roughness in turning of high-alloy white cast iron. *Measurement*. 2013;46(2): 913–919. https://doi.org/10.1016/j.measurement.2012.10.013
**20.** Nalbant M., Gökkaya H., Sur G. Application of Taguchi method in the optimization of cutting parameters for surface roughness in turning. *Materials and Design*. 2007; 28(4):1379–1385. https://doi.org/10.1016/j.matdes.2006.01.008
**21.** Krakhmalev P., Yadroitsava I., Fredriksson G., Yadroitsev I. *In situ* heat treatment in selective laser melted martensitic AISI 420 stainless steels. *Materials and Design*. 2015;87:380–385. https://doi.org/10.1016/j.matdes.2015.08.045
**22.** Ghani J.A., Choudhury I.A., Hassan H.H. Application of Taguchi method in the optimization of end milling parameters. *Journal of Materials Processing Technology*. 2004;145(1): 84–92. https://doi.org/10.1016/S0924-0136(03)00865-3
**23.** Danielsoper.com. "Critical F-value Calculator". Available at URL: https://www.danielsoper.com/statcalc/calculator.aspx (Accessed: 15.02.2025).

## Information about the Authors / Сведения об авторах

***Cinzhun Zhang,*** *Postgraduate of the Chair of Mechanical Engineering*, National Research Tomsk Polytechnic University
***ORCID:*** 0009-0002-7820-1227
***E-mail:*** cinzhun1@tpu.ru

***Viktor N. Kozlov,*** *Cand. Sci. (Eng.), Assist. Prof. of the Department of Mechanical Engineering of the Engineering School of New Production Technologies*, National Research Tomsk Polytechnic University
***ORCID:*** 0000-0001-9351-5713
***E-mail:*** kozlov-viktor@bk.ru

***Dmitrii A. Chinakhov,*** *Dr. Sci. (Eng.), Dean of the Aircraft Faculty*, Novosibirsk State Technical University
***ORCID:*** 0000-0002-4319-7945
***E-mail:*** chinakhov@corp.nstu.ru

***Vasilii A. Klimenov,*** *Dr. Sci. (Eng.), Prof.-Consultant of the Department of Materials Science of the Engineering School of New Production Technologies*, National Research Tomsk Polytechnic University
***ORCID:*** 0000-0001-7583-0170
***E-mail:*** klimenov@tpu.ru

***Roman V. Chernukhin,*** *Cand. Sci. (Eng.), Assist. Prof. of the Chair of Engineering of Technological Machines*, Novosibirsk State Technical University
***ORCID:*** 0000-0003-1324-0161
***E-mail:*** chernuxin@corp.nstu.ru

***Цинжун Чжан,*** *аспирант кафедры машиностроения*, Национальный исследовательский Томский политехнический университет
***ORCID:*** 0009-0002-7820-1227
***E-mail:*** cinzhun1@tpu.ru

***Виктор Николаевич Козлов,*** *к.т.н., доцент отделения машиностроения Инженерной школы новых производственных технологий*, Национальный исследовательский Томский политехнический университет
***ORCID:*** 0000-0001-9351-5713
***E-mail:*** kozlov-viktor@bk.ru

***Дмитрий Анатольевич Чинахов,*** *д.т.н., декан факультета летательных аппаратов*, Новосибирский государственный технический университет
***ORCID:*** 0000-0002-4319-7945
***E-mail:*** chinakhov@corp.nstu.ru

***Василий Александрович Клименов,*** *д.т.н., профессор-консультант отделения материаловедения Инженерной школы новых производственных технологий*, Национальный исследовательский Томский политехнический университет
***ORCID:*** 0000-0001-7583-0170
***E-mail:*** klimenov@tpu.ru

***Роман Владимирович Чернухин,*** *к.т.н., доцент кафедры проектирования технологических машин*, Новосибирский государственный технический университет
***ORCID:*** 0000-0003-1324-0161
***E-mail:*** chernuxin@corp.nstu.ru

## Contribution of the Authors / Вклад авторов

***C. Zhang*** – conducting experimental studies, applying the Taguchi method for analysis of variance, data processing, writing the text.

***V. N. Kozlov*** – conducting experiments and analyzing the causes of changes in strength depending on processing parameters, writing the text.
***D. A. Chinakhov*** – final editing of the article, data processing.

***V. A. Klimenov*** – writing the text, analysis and data processing.

***R. V. Chernukhin*** – systematization and processing of experimental data.

***Ц. Чжан*** – проведение экспериментальных исследований, применение метода Тагучи для дисперсионного анализа, обработка данных, написание текста статьи.
***В. Н. Козлов*** – проведение экспериментов и анализ причин изменения силы в зависимости от параметров обработки, написание текста статьи.
***Д. А. Чинахов*** – окончательное редактирование статьи, обработка данных.
***В. А. Клименов*** – написание текста статьи, анализ и обработка данных.
***Р. В. Чернухин*** – систематизация и обработка экспериментальных данных.

Received 14.03.2025
Revised 01.09.2025
Accepted 10.09.2025

Поступила в редакцию 14.03.2025
После доработки 01.09.2025
Принята к публикации 10.09.2025